

1 **Atmospheric Speciated Mercury Concentrations on an Island between China and Korea:**
2 **Sources and Transport Pathways**

3

4 **Gang-San Lee¹, Pyung-Rae Kim¹, Young-Ji Han^{1,11}, Thomas M. Holsen², Yong-Seok Seo^{3,4},**
5 **Seung-Muk Yi³**

6

7 ¹Department of Environmental Science, College of Natural Science, Kangwon National University, 1
8 Kangwondaehak-gil, Chuncheon, Kangwon-do, 200-701, Republic of Korea

9 ²Department of Civil and Environmental Engineering, Clarkson University, 8 Clarkson Ave., Potsdam,
10 NY 13699-5710, USA

11 ³Department of Environmental Health, Graduate School of Public Health, Seoul National University,
12 Gwanak-ro, Gwanak-gu, Seoul 151-742, Republic of Korea

13 ⁴Institute of Health and Environment, Seoul National University, 1 Gwanak-ro, Gwanak-gu, Seoul
14 151-742, Republic of Korea

15

16

17

18

19

20

21

22

23

24

25

26

¹ Correspondence to: Y.J. Han (youngji@kangwon.ac.kr)

27 **Abstract**

28 As a global pollutant, mercury (Hg) is of particular concern in East Asia where anthropogenic
29 emissions are the largest. In this study, speciated Hg concentrations were measured on Yongheung
30 Island, the western most island in Korea, located between China and the Korean mainland to identify
31 the importance of local and regional Hg sources. Various tools including correlations with other
32 pollutants, conditional probability function, and back-trajectory based analysis consistently indicated
33 that Korean sources were important for gaseous oxidized mercury (GOM) whereas, for total gaseous
34 mercury (TGM) and particulate bound mercury (PBM), regional transport were also important. A
35 trajectory cluster based approach considering both Hg concentration and the fraction of time each
36 cluster was impacting the site was developed to quantify the effect of Korean sources and out-of-
37 Korean source. This analysis suggests that contributions from out-of-Korean sources were similar to
38 Korean sources for TGM whereas Korean sources contributed slightly more to the concentration
39 variations of GOM and PBM compared to out-of-Korean sources. The ratio of GOM/PBM decreased
40 when the site was impacted by regional transport, suggesting that this ratio may be a useful tool for
41 identifying the relative significance of local sources vs. regional transport. The secondary formation
42 of PBM through gas-particle partitioning with GOM was found to be important at low temperatures
43 and high relative humidity.

44

45 **Keywords** : *TGM, GOM, PBM, regional transport, gas-particle partitioning, cluster analysis*

46

47 **1. Introduction**

48

49 Mercury (Hg) is the only metal that exists as a liquid at standard conditions (US EPA, 1997) which
50 results in it having a significant vapor pressure and presence in the atmosphere. In the atmosphere, Hg
51 generally does not constitute a direct public health risk at the level of exposure usually found (Driscoll
52 et al, 2007). However, once Hg is deposited into aquatic systems, it can be transformed into methyl-
53 mercury (MeHg) which is very toxic and readily bioaccumulates through the food web (Mason et al.,

54 1995). Many studies show that one of the major sources of MeHg in aquatic and terrestrial system is
55 atmospheric deposition of inorganic Hg (Landis and Keeler, 2002, Mason et al., 1997). Fish
56 consumption has been considered to be the major exposure pathway of Hg for humans (Mergler et al.,
57 2007; UNEP, 2013). In Korea, You et al. (2012) showed that MeHg concentrations in blood were
58 affected by fish consumption as well as by gender difference. However, rice consumption was also
59 found to be the predominant pathway of MeHg exposure for the inhabitants residing in a highly
60 contaminated area of China (Zhang et al., 2010).

61 Atmospheric mercury exists in three major inorganic forms, including gaseous elemental mercury
62 (GEM, Hg^0), gaseous oxidized mercury (GOM, Hg^{2+}) and particulate bound mercury (PBM, $\text{Hg}(p)$).
63 The sum of the GEM and GOM is often called as total gaseous mercury (TGM). Due to its high water
64 solubility and deposition velocity, GOM has short atmospheric residence times (~day) and,
65 consequently, its ambient concentration is mainly affected by local sources. Besides the anthropogenic
66 sources, the free troposphere has been identified as an important GOM source (Huang and Gustin,
67 2012; Weiss-Penzias et al., 2009; Timonen et al., 2013). In contrast, GEM, which comprises more
68 than 95 percent of the total Hg in ambient air, can be transported long distances because it is relatively
69 inert and has low water solubility and deposition velocity (Lin and Pehkonen, 1999). The residence
70 time of PBM is dependent on the size of associated particles, but generally, it has been assumed to be
71 a few days (Fang et al., 2012, Zhang et al., 2001). Measurements of GOM and PBM are challenging
72 and uncertain due to their extremely low concentrations and complex chemical reactivity, and because
73 their chemical forms are not actually known (Pirrone et al., 2013). In most studies, GOM and PBM
74 have operational definitions for the mercury species collected by a KCl coated denuder and by a
75 quartz filter downstream of a KCl denuder, respectively. It is typically assumed that GOM comprises
76 HgCl_2 , HgBr_2 , HgO , $\text{Hg}(\text{NO}_3)_2$, and HgSO_4 . However, the sampling method including the use of a
77 KCl denuder has been shown to be subject to interferences from ozone, water vapor and possibly
78 other compounds (Lyman et al. 2010; Talbot et al., 2011; Jaffe et al., 2014; Finley et al., 2013; Gustin
79 et al., 2013; Huang et al., 2013; McClure et al., 2014), and it also should be noted that the different
80 $\text{Hg}(\text{II})$ compounds have different collection efficiencies by the KCl coated denuder (Gustin et al.,

81 2015).

82 In the atmosphere, Hg species can be interconverted through various redox reactions. It is known
83 that GOM can be produced by homogeneous and heterogeneous reactions of GEM with O₃, OH, and
84 Br/BrO (Hedgecock and Pirrone, 2004; Obrist et al., 2011; Subir et al., 2011), but there is no
85 consensus on which oxidants are most important under which environmental conditions. GEM can
86 also be formed through reduction of GOM predominantly in cloud water (Subir et al. 2011, 2012).
87 GOM can also be converted to PBM through gas-particle partitioning, with the partition coefficient,
88 K_p, inversely correlated with temperature and positively correlated with particle surface area (Lyman
89 and Keeler, 2005, Rutter and Schauer, 2007a,b; Liu et al., 2010). Since GEM makes up the bulk of the
90 total Hg in ambient air its formation through reduction processes of divalent Hg may not be important.
91 However, the secondary formations of GOM through the oxidation of Hg⁰ followed by gas-particle
92 partitioning formation of PBM can contribute significantly to their ambient concentrations.

93 The region of largest anthropogenic Hg emissions is East and Southeast Asia, contributing 39.7%
94 of the total global anthropogenic emissions (UNEP, 2013). In Korea, atmospheric Hg emissions have
95 generally decreased since 1990 (Kim et al., 2010). However, Hg levels in Korea are likely to be
96 highly susceptible to Chinese emissions because China alone accounts for about one third of the
97 global total (UNEP, 2013) and Korea is situated just east (and generally downwind) of China.
98 According to the recent studies, Hg concentrations in blood of Koreans are more than 4~8 times
99 higher than those found in US and Germany, and approximately 26% of Koreans have higher blood
100 mercury concentrations than a USA guideline level (<http://envhealth.nier.go.kr>), indicating that there
101 is an urgent need to identify the Hg sources and pathways controlling Hg concentrations in Korea.

102 This study was designed to identify the contribution of various Hg sources including direct
103 emissions from anthropogenic and natural sources and indirect secondary formation processes to
104 atmospheric Hg concentrations in Korea. In order to achieve these objectives, Hg concentrations were
105 measured in the western most island in Korea, located in between eastern China and the Korean
106 mainland, so that, depending on wind patterns, the effects of Chinese and Korean Hg emissions could
107 be evaluated. Previously, our group qualitatively evaluated the impact of local Korean sources and

108 regional Chinese sources on TGM concentrations at the same sampling site (Lee et al. 2014).
109 However, that work was unable to identify the effect of sources on Hg levels in Korea because only
110 TGM was measured whereas all three Hg species are needed since they have very different physical
111 and chemical properties. In this study, the importance of sources and pathways were both qualitatively
112 and quantitatively evaluated using all three Hg species' concentrations measured throughout the
113 extended sampling period.

114

115 **2. Materials and methods**

116 **2.1 Site description**

117 TGM, GOM and PBM were measured on the roof of a three-story building on Yongheung Island
118 (YI), the westernmost island in Korea (Fig. 1). YI is a small island located about 15~20 km west from
119 mainland Korea with a population of 5,815. The Yongheung Coal-fired Power Plant (YCPP), located
120 approximately 4.5 km southwest of the sampling site (Fig 1c), emits about 0.11 ton yr⁻¹ of Hg. To the
121 east of the sampling site, industrial (the Incheon industrial complex shown as light violet color in Fig
122 1b and Fig 1c) and metropolitan (Seoul shown as a pink color in Fig 1b and Fig 1c) areas are located
123 in mainland Korea, and, in the southern direction, there are three large coal fired power plants (Fig 1b).
124 The Hg emission rate of anthropogenic sources in Korea was estimated to be 8.04 ton yr⁻¹ in 2010,
125 with cement production being the largest source type (AMAP/UNEP, 2013).

126

127 **2.2 Sampling and analysis**

128 From January 2013 to August 2014, three atmospheric mercury species: TGM (GEM+GOM), GOM,
129 and PBM ($\leq 2.5 \mu\text{m}$) were measured during eight intensive sampling periods (Table 1). TGM
130 concentrations were measured every 5 min using a mercury vapor analyzer (Tekran 2537B). This
131 instrument contains two gold cartridges which collect and thermally desorb Hg alternately. Desorbed
132 Hg is quantified using cold vapor atomic fluorescence spectrometry (CVAFS). Outdoor air at a flow
133 rate of 1.0 L min⁻¹ was transported through a 3-m-long heated sampling line (1/4" OD Teflon) into the
134 analyzer. There is a possibility that some of GOM may be sorbed in the line upstream of the gold traps

135 although the sampling line and inlet were maintained at 50°C to prevent the GOM sorption. However,
136 it is typically assumed that Tekran 2537 can collect and analyze TGM in most of studies (Temme et al.,
137 2002; Gustin et al., 2013; Han et al., 2014; Zhang et al., 2015). The Tekran 2537B was automatically
138 calibrated daily using an internal permeation source. Manual injections were also used to evaluate
139 these automated calibrations before each sampling campaign using a saturated mercury vapor
140 standard. The relative percent difference between manual injection and automated calibration was
141 <2%. Five-point manual calibration was also performed by injecting Hg vapor into the sampling line
142 two times during the study period. The R² ranged from 0.9991 to 0.9997 between mass injected and
143 Tekran reported area, and the average relative percent difference between the mass injected and the
144 mass calculated was 5.5%. The method detection limit (0.04 ng m⁻³) was calculated as three times the
145 standard deviation obtained after injecting 1 pg of the mercury vapor seven times. The recovery rate
146 (96 ± 3%) was obtained by directly injecting Hg vapor into the sampling line between the sample inlet
147 and the Tekran 2537B in a zero-air stream.

148 GOM and PBM were collected manually using an annular denuder coated with KCl followed by a
149 quartz filter, respectively, at a flow rate of 10 L min⁻¹. To identify any diurnal variations, all samples
150 were separately collected during the daytime (07:00-19:00) and nighttime (19:00-07:00) except during
151 the 7th sampling period when they were measured every 2 hrs. The sampling system including an
152 elutriator, an impactor, a KCl-coated denuder and a filter pack was housed in a custom-made sampling
153 box maintained at 45°C to prevent hydrolysis of KCl. After sampling, the denuder and quartz filter
154 were thermally desorbed using a tube furnace at 525°C and 900°C, respectively, to convert Hg²⁺ to
155 Hg⁰ in a carrier gas of zero air. The heated air was then transported into a Tekran 2537B for
156 quantification. Field blanks for GOM and PBM were collected once for each sampling period, and
157 their average values were 0.23 ± 0.12 pg m⁻³ and 0.25 ± 0.09 pg m⁻³, respectively.

158 The sampling methods used in this study are currently the most accepted methods for the
159 measurement of atmospheric GOM and PBM, however there are many studies reporting that these
160 methods are subject to interferences from ozone, water vapor and possibly other compounds (Lyman
161 et al. 2010; Talbot et al., 2011; Jeff et al., 2014; Finley et al., 2013; Gustin et al., 2013; Huang et al.,

162 2013; McClure et al., 2014) although recent side-by-side measurements with two Tekran systems
163 showed good agreement and no impact from added ozone and increasing relative humidity (Edgerton,
164 personal communication). Also, it should be noted that the concentrations of PBM measured during
165 12-hrs of sampling time (all sampling periods except in the 7th) may have been biased due to Hg loss
166 from filters over the long sampling period; however for model development any loss of PBM is
167 assumed to be the same for each sampling period. Therefore, it should be noted that the GOM and
168 PBM measurements reported in this study may be somewhat biased even though, at present, it is not
169 possible to quantify the magnitude of these uncertainties.

170 Meteorological data including temperature, wind speed, wind direction, relative humidity and solar
171 radiation were also measured every 5 min at the sampling site using a meteorological tower (DAVIS
172 Inc weather station, Vintage Pro2TM).

173 Hourly concentrations of SO₂, NO₂, CO, O₃ and PM₁₀ were obtained from the national air quality
174 (NAQ) monitoring station (<http://www.airkorea.or.kr/>) located approximately 8 km east from the
175 sampling site. These concentrations were compared with those measured at another national air
176 quality monitoring station located approximately 24 km west of the Hg sampling site, and there were
177 no statistical differences between sites (p-value < 0.001), indicating that the spatial distribution of
178 these pollutants was relatively uniform across the area

179

180 **2.3. Backward trajectory and Cluster analysis**

181 Three-day backward trajectories were calculated using the NOAA HYSPLIT 4.7 with GDAS
182 (Global Data Assimilation System) meteorological data which supplies 3-hour, global 1 degree
183 latitude-longitude datasets of the pressure surface. Hourly 3-day back-trajectories were calculated for
184 each hour of sampling, and the arrival heights of both 200 m and 500 m were used to describe the
185 local and the regional transport meteorological pattern. Since GOM and PBM were measured for 12hr
186 for most time periods, hourly trajectories were matched to the 12hr-averaged GOM and PBM
187 concentration; therefore, in total 12 back-trajectories represented one averaged GOM or PBM
188 concentrations. **Although there have been many studies using different time scales for measurements**

189 of pollutants and for meteorological data (Amato and Hopke, 2012; Galindo et al., 2011; Kim et al.,
190 2007) this mismatch might increase the uncertainty for the trajectory-based approaches.

191 The backward trajectories were clustered into groups with similar transport patterns using NOAA
192 HYSPLIT 4.7. This method minimizes the intra-cluster differences among trajectories while
193 maximizing the inter-cluster differences. The clustering of trajectories is based on the total spatial
194 variance (TSV) method. TSV is the sum of all the cluster spatial variances (SPVAR) which is the sum
195 of the squared distances between the endpoints of the cluster's component trajectories and the mean of
196 the trajectories in that cluster. In this study, five clusters were chosen based on a large increase in TSV
197 for larger clusters (Fig. 4S), as described in Draxler et al. (2014) and Kelly et al. (2012). A more
198 detailed description of the clustering process can be obtained in Draxler et al. (2014).

199

200 **2.5. Conditional Probability Function (CPF)**

201 The conditional probability that a given concentration from given wind direction will exceed a
202 predetermined threshold criterion, was calculated using the following equation.

$$203 \quad \text{CPF}_{\Delta\theta} = \frac{m_{\Delta\theta}}{n_{\Delta\theta}} \quad (\text{Eq.1})$$

204 where $m_{\Delta\theta}$ is the number of occurrences from wind sector $\Delta\theta$ where the concentration is higher than a
205 criterion value, and $n_{\Delta\theta}$ is the total number of occurrence from this wind sector. In this study, 16
206 sectors were used ($\Delta\theta = 22.5^\circ$), and calm winds were excluded from the calculation because of
207 isotropic behavior of the wind vane for such conditions. For TGM, two threshold criteria of the upper
208 10 and 25 percentile were chosen while only the upper 25 percentile was used for GOM and PBM
209 concentrations due to the smaller number of samples. The 1hr-averaged wind direction (WD) data
210 were used for 12hr-averaged GOM and PBM concentrations for most of periods, so that in total 12
211 WS and WD were used for one averaged GOM and PBM concentrations to create CPF. **It should be**
212 **noted that there are some unquantifiable uncertainties derived from using different time resolutions**
213 **between measurements of GOM and PBM and WD data although overall trajectories did not diverge**
214 **significantly at this sampling site for most sampling periods.**

215

216 2.6. Potential Source Contribution Function (PSCF)

217 The PSCF model counts each trajectory segment endpoint that terminates within given grid cell. A
218 high PSCF value signifies a potential source location. The PSCF value was calculated as:

$$219 \text{ PSCF value} = \frac{P[B_{ij}]}{P[A_{ij}]} = \frac{m_{ij}}{n_{ij}} \quad (\text{Eq.2})$$

220 If N is the total number of trajectory segment endpoints over the study period and if n segment
221 trajectory endpoints fall into the ij th cell, the probability of this event ($P[A_{ij}]$) is calculated by n_{ij}/N . If
222 m_{ij} is the number of segment endpoints in the same ij th cell when the concentrations are higher than a
223 criterion value, the probability of this high concentration event, B_{ij} , is given by $P[B_{ij}] = m_{ij}/N$. The
224 criterion value was the top 25% concentration and the cell size of 0.5° by 0.5° was used for tracing
225 sources. To reduce the uncertainty in a grid cell with a small number of endpoints, an arbitrary weight
226 function W_{ij} was applied when the number of the endpoints in a particular cell was less than three
227 times the average number of endpoints (N_{ave}) for all cells (Fu et al., 2011, Han et al., 2007, Polissar et
228 al., 2001a, 2001b).

$$229 W_{ij} = \begin{pmatrix} 1.0 & N_{ij} > 3N_{ave} \\ 0.70 & 3N_{ave} > N_{ij} > 1.5N_{ave} \\ 0.40 & 1.5N_{ave} > N_{ij} > N_{ave} \\ 0.20 & N_{ave} > N_{ij} \end{pmatrix} \quad (\text{Eq. 3})$$

230 In this study, trajectories were hourly calculated

231

232 3. Results and discussion

233 3.1. General trends of three Hg species

234 To maintain the consistency of the sampling duration, the 12hr-averaged GOM and PBM
235 concentrations were used for the 7th sampling period to identify the general trends of Hg species. The
236 average TGM, GOM, and PBM concentrations were $2.8 \pm 1.1 \text{ ng m}^{-3}$, $8.3 \pm 9.7 \text{ pg m}^{-3}$, and $10.9 \pm$
237 11.2 pg m^{-3} , respectively (Table 1). Since the GOM concentration was much lower than TGM the
238 reported TGM concentration can be considered a good approximation of the GEM concentration.
239 TGM varied from 0.1 to 18.8 ng m^{-3} ; the highest concentration was observed around 2 am on March
240 18, 2014 (Fig. 2). GOM and PBM concentrations peaked at 50.9 pg m^{-3} during the daytime on March

241 19, 2014 and 43.7 pg m^{-3} during daytime on January 22, 2013, respectively (Fig. 2). The various Hg
242 species did not follow similar concentration patterns although PBM was statistically significantly
243 correlated with TGM (Pearson correlation coefficient, $r= 0.235$, $p\text{-value}= 0.03$).

244 When the data were grouped into three categories including the first (Apr., 2013, May, 2013, Mar.,
245 2014, May, 2014), the second (Aug, 2013, Aug., 2014.), and the third (Jan., 2013, Feb., 2013) periods,
246 both TGM (ANOVA/Tukey test, $p\text{-value}<0.001$) and PBM ($p\text{-value}=0.024$, Kruska-Wallis test) had
247 the highest concentrations in cold period ((Jan., 2013, Feb., 2013) while there was no statistical
248 difference in GOM concentrations among different categories ($p\text{-value}= 0.288$, Kruskal-Wallis test)
249 (Fig. 3). Observed TGM concentrations were substantially lower than those measured in a suburban
250 and remote site in China and metropolitan areas of Korea (Seoul), but higher than at most North
251 American sites and at a rural site of Korea (Chuncheon) (Table 2). GOM and PBM concentrations
252 were in between those typically found at urban locations and at a rural site in Korea and were much
253 lower than those typically measured in China.

254 The TGM concentration varied diurnally, generally showing morning maximums (07:00-12:00) and
255 minimums during the nighttime. In urban areas, TGM concentrations are typically higher during the
256 nighttime due to a combination of decreased GEM loss by daytime oxidation, increased use of
257 household heating systems and decreased mixing heights at night (Kim et al., 2012; Han et al., 2014).
258 In contrast daytime peaks have been observed in rural and remote areas, likely due to increased
259 volatilized of Hg^0 from natural sources (Choi et al., 2008; Cheng et al., 2014). Overall these results
260 suggest that TGM concentrations at this site are elevated due to the proximity of regional sources and
261 daily variations are controlled by natural emissions from the ocean and soil surfaces.

262 GOM concentrations were the highest in spring ($10.7 \pm 10.1 \text{ pg m}^{-3}$) and the lowest in summer
263 ($6.2 \pm 4.9 \text{ pg m}^{-3}$) with statistically insignificant seasonal variation (Fig. 3). The lack of a GOM
264 seasonal variation for could be an indicator of insignificant secondary formation through
265 photochemical oxidation reactions, but it might be also be due to the small sample numbers and/or
266 relatively long sampling duration (12hr). PBM concentrations did have statistically significant
267 seasonal variations with the highest average concentration in winter ($17.8 \pm 16.7 \text{ pg m}^{-3}$) and the lowest

268 average concentration in summer ($5.8 \pm 4.1 \text{ pg m}^{-3}$) (Fig. 3). Higher PBM concentrations in winter
269 were likely caused by increased biomass burning and residential heating, decreased removal from the
270 atmosphere due to the lower precipitation depth, and/or lower temperatures which favor partitioning
271 to the aerosol phase. Previous studies also often observed the highest PBM concentrations in winter
272 (Mao et al., 2012; Amos et al., 2012; Lan et al., 2012).

273 In Korea emissions of PBM from anthropogenic sources are much smaller than gaseous emissions
274 (the proportion of GEM, GOM, and PBM released are 64.4%, 28.8%, and 6.8%)(Kim et al., 2010).
275 The fact that PBM concentrations are similar to GOM even though significantly less PBM is released
276 suggests that a significant portion of atmospheric PBM may be due to secondary formation through
277 gas-particle partitioning. This process is characterized by a partition coefficient, K_p , which is inversely
278 correlated with temperature (Rutter and Schauer, 2007), possibly causing the distinct seasonal
279 variation in PBM concentrations at the sampling site.

280 The relationship between K_p , defined as:

$$281 \quad K_p = \frac{PBM/PM}{Hg_{gas}} \quad (\text{Eq. 4})$$

282 where PM represents the particle mass, and Hg_{gas} is the concentration of gaseous Hg and relative
283 humidity (RH) was examined (PM10 concentration was used for PM in Eq. 4 in this study). RH was
284 included since in recent studies K_p was found to increase at high relative humidity in colder seasons
285 (Lyman and Keeler, 2005; Liu et al., 2010). Note that the sampling site was located in a coastal area
286 with generally high RH.

287 Some previous studies suggested that all gaseous mercury species including Hg^0 may deposit on
288 particles (Xiu et al., 2005; 2009); however, others suggested that the gas-particle partitioning of GOM
289 occurred but assumed that the adsorption of Hg^0 on particles was negligible due to its high vapor
290 pressure (Amos et al., 2012; Rutter and Schauer, 2007). Consistent with this hypothesis, we found a
291 statistically significant multiple linear relationship between K_p with temperature and relative humidity
292 (Fig. 4):

$$293 \quad \text{Log}(K_p) = -2.518 - 0.036(T) + 0.017(RH) \quad (\text{Eq. 5})$$

294 where T and RH indicate atmospheric temperature ($^{\circ}\text{C}$) and relative humidity (%), respectively. The

295 multiple linear equation fit the data well ($R^2=0.29$, $R=0.54$, $p\text{-value}<0.001$), and both variables of
 296 temperature and relative humidity were statistically significant ($p\text{-value}<0.001$). The partial
 297 correlation coefficients were -0.389 for temperature ($p\text{-value}<0.001$) and 0.375 for RH ($p\text{-}$
 298 $\text{value}=0.001$). When each of the temperature and the RH was used as a single independent variable
 299 the $\log(K_p)$ regression equation was still significant with a Pearson correlation coefficient of -0.42
 300 ($R^2=0.18$, $p\text{-value}<0.001$) and 0.39 ($R^2=0.15$, $p\text{-value}<0.001$), somewhat lower than that from the
 301 multiple regression (Fig. 1S). Amos et al. (2012) found an empirical gas-particle partitioning
 302 relationship between K_p and T using the Hg data obtained from five monitoring sites in United States
 303 and Canada and two laboratory experiments, and average equation is :

$$\text{Log}(1/K_p) = (10 \pm 1) - (2500 \pm 300)/T \quad (\text{Eq. 6})$$

304 where T is in Kelvin unit. When a partial linear regression was performed with T in this study similar
 305 equation was derived: $\text{Log}(1/K_p) = 13.5 - 3362.7/T$. In Amos et al. (2012), the coefficients, β and y_0 ,
 306 ranged from -1600 to -3300 and 6 to 13 , respectively, and R^2 ranged from 0.16 to 0.57 in different
 307 monitoring sites. Rutter and Schauer (2007a) also determined the relationship between $\text{Log}(1/K_p)$ for
 308 urban aerosols with inverse temperature and found the slope and intercept were -4250 ± 480 and 10 ± 2 ,
 309 respectively, with R^2 of 0.77 . Another study using datasets from 10 AMNet sites located in North
 310 America found R^2 ranged between 0.04 and 0.53 . In summary the values derived in this study fall
 311 between those reported by other studies. Somewhat lower R^2 in this study is probably caused by
 312 smaller number of samples, different composition of aerosol, different GOM species, and/or longer
 313 sampling duration.

315 Han et al. (2014) also found a significant multiple linear relationship between the ratio of
 316 PBM/GOM with temperature and relative humidity at a rural site ($R^2=0.613$, β for T= -0.774 , β for
 317 RH= 0.33) but not at an urban site. The lower correlation coefficient and the beta values found in this
 318 study compared to those from Han et al. (2014) is probably due to the greater impact of primary
 319 anthropogenic sources around the sampling site. A large anthropogenic source near the sampling site
 320 is likely to weaken the relative contribution of gas-particle partitioning (secondary formation) to the
 321 variations of ambient PBM and GOM concentration because both Hg species can be also strongly

322 affected by the primary source emission. In the study of Amos et al. (2012), the highest R^2 was shown
323 in Experimental Lakes Area of Canada and Reno, NV where no large anthropogenic sources of Hg is
324 located.

325 In previous researches, GOM concentration measured using KCl denuder is subject to interferences
326 under the conditions of high ozone and relative humidity (Gustin et al., 2012; Huang et al., 2013;
327 Gustin et al., 2015) although it is currently the most accepted method. To evaluate the possible error
328 on interpreting result, K_p was re-calculated with re-calculated GOM concentration using the empirical
329 equation suggested by McClure et al. (2014) ($RH=0.63 \text{ GOM loss \%} + 18.1$). Since McClure et al.
330 (2014) suggested this equation at RH of 21 to 62%, the GOM concentrations collected only when RH
331 was from 20% to 65% were re-calculated. The multi-linear relationship was compared between re-
332 calculated K_p and original K_p , and the results were very similar to each other (Fig. 2S).

333

334 **3.2. Tracing sources of Hg species**

335 Correlations between Hg and other pollutant concentrations are often used to identify sources. For
336 example good correlations with SO_2 and CO typically indicate the impact of coal combustion (Pirrone
337 et al., 1996; Han et al., 2014), and a strong correlation between Hg and CO has often been used as an
338 indicator for regional transport because both pollutants have similar sources and do not easily
339 decompose by reaction and undergo deposition during transport (Weiss-Penzias et al., 2003, 2006;
340 Kim et al., 2009) although a few recent studies showed the significant bromine-induced oxidation of
341 GEM in the mid-latitude marine boundary layer as well as in the polar atmosphere (Ariya, 201; Obrist
342 et al., 2011). A good correlation between Hg and NO_2 suggests the site is being impacted by local
343 sources because the lifetime of NO_2 is relatively short compared with that of CO (Seinfeld and Pandis,
344 2006). In this study TGM concentrations were well correlated with SO_2 , CO, and PM_{10} concentrations
345 but not with NO_2 concentrations (Table 3), indicating that regional transport of TGM emitted from
346 coal combustion was impacting the site throughout much of the sampling period. PBM concentrations
347 also had a statistically significant relationship with TGM and CO suggesting regional transport is also
348 important for PBM, but GOM was not correlated with any other pollutant suggesting it is impacted to

349 a greater extend by local sources (see additional discussion below).

350 CPF plot shows that the top 25% TGM concentrations were associated with winds from the NNW
351 and eastern direction, pointing towards northeastern China and inland Korean sources; however, when
352 the criterion was set to the top 10% the winds from NNW became less important and the sources
353 located in southern and eastern areas from the sampling site were identified as an important source
354 direction (Fig. 5). The CPF plot for GOM is significantly different from the one for PBM. High PBM
355 concentrations were associated with northern winds while GOM concentrations were enhanced during
356 southeastern winds.

357 These results suggest that for PBM regional transport from Chinese and North Korea sources were
358 more important than Korean sources; in contrast coal fired power plants located in the southern
359 direction rather than regional transport impacted GOM concentration. It should be noted that this
360 result is in apparent conflict with the finding that there was no relationship between GOM and SO₂
361 concentrations. Total SO₂ emissions from power plants in China (18.6 Tg yr⁻¹) are much larger than in
362 Korea (0.09 Tg yr⁻¹), and SO₂ emission rates per capita and per area in China also greatly surpass
363 those in Korea (Lu et al., 2010). Much larger SO₂ emissions in China raise the background SO₂
364 concentration in the region and may mask any correlation between GOM and SO₂ even if coal fired
365 power plants located in the southerly direction from the sampling site impacted GOM concentrations.
366 In support of this hypothesis the pollution rose indicates that high SO₂ concentrations are associated
367 with westerly winds while high GOM concentrations are associated with southerly winds. It should be
368 noted that only the top 25% of GOM and PBM concentrations were used as the criteria for the CPF
369 plot because the number of samples for both species were significantly less than for TGM due to their
370 longer sampling duration (12hr).

371 Among the eight sampling periods, the second period (April, 2013) had the highest TGM, PBM and
372 the second highest GOM average concentration, and SO₂, NO₂, CO, and PM10 were also quite high
373 (Table 1). During this period, TGM was statistically well correlated with SO₂ (r= 0.55), NO₂ (r=0.56),
374 and CO (r=0.36), with the highest Pearson correlation coefficient with NO₂, the characteristic local
375 pollutant. In addition, the CPF plot (for TGM) and the back-trajectories were also associated with

376 easterly winds transporting air masses from major Korean urban areas, supporting the previous
377 suggestion that inland sources enhanced all three Hg concentrations during the second sampling
378 period.

379 In contrast the fifth sampling period had the lowest GOM, PBM and the second lowest TGM
380 concentrations (Table 1). Note however that the TGM concentrations for the first couple of days
381 reached approximately 5 ng m^{-3} and gradually decreased to about 1 ng m^{-3} during the last days of
382 sampling (Fig. 2), indicating that there was likely two different sources affecting Hg concentrations
383 during this period. Back-trajectories associated with high TGM concentrations passed through
384 northeastern China, North Korea and the industrial/metropolitan areas of Korea before arriving at the
385 sampling site whereas trajectories during the low TGM concentrations spent long periods within the
386 ocean boundary layer. Although Hg can be emitted from ocean surface (Han et al., 2007; UNEP, 2013)
387 heavy rain and low solar radiation occurring during the last two days of this period probably inhibited
388 emissions of Hg from the ocean surface.

389

390 **3.2.1 GOM/PBM ratio**

391 According to the CPF results, the winds from NW and NE of the sampling site were responsible for
392 the elevated PBM concentrations while easterly winds pointing towards inland Korea were associated
393 with increased GOM concentrations (Fig. 5). The finding that regional transport of TGM and PBM to
394 the site is important is supported by their significant correlation with CO (Table 3). In order to
395 identify the relative importance of local sources relative to regional transport, the ratio of GOM/PBM
396 was used as an indicator because the atmospheric residence time of GOM is widely regarded to be
397 shorter than that of PBM (even though there is no consensus on what specific chemical forms are
398 collected by KCl-coated denuders). The GOM/PBM ratio should be higher if local sources are more
399 important, and the GOM/PBM ratio is likely to decrease as regional transport becomes more
400 important. In this study the GOM/PBM ratios were categorized into three groups: low (0~2), middle
401 (2~8), and high (>8) and the frequency of wind direction was compared (Fig. 6). The result clearly
402 indicates that the southerly and southeasterly winds were associated with high GOM/PBM ratios and

403 that the westerly and northerly winds indicative of regional transport from China prevailed at lower
404 GOM/PBM ratios. There was a weak negative correlation between the ratio of GOM/PBM and CO
405 concentration at a significance level of 0.1 (p-value= 0.089) (Fig. S3), supporting the assertion that the
406 GOM/PBM ratio decreased with the increased effect of regional transport. Lynam and Keeler (2005)
407 also found that high GOM/PBM ratio was observed with influences from local sources and low
408 GOM/PBM ratios appeared with influence from regional sources in Detroit. In Korea, Kim et al.
409 (2009) found a significant increase in the PBM/GOM ratio during high PM_{2.5} concentration events
410 caused by regional transport from China.

411 The reciprocal of this ratio (i.e. GOM/PBM) was used to calculate K_p which indicates that the
412 secondary formation of PBM through gas-particle partitioning was became more important as the
413 significance of regional transport increased, suggesting that secondary production was favored when
414 air underwent regional transport, as has been shown previously (Lynam and Keeler, 2005). **It should**
415 **be noted that there are uncertainties related to different aerosol composition, particle surface area**
416 **variations, and/or temperature change which can affect both K_p and the GOM/PBM ratio.**

417

418 **3.2.2 PSCF results**

419 In order to locate potential source areas in more detail, PSCF was used. For TGM, potential sources
420 were located in Liaoning, Shandong, and Henan provinces of China along with the southern area of
421 Korea (Fig. 7). Liaoning province, where large non-ferrous smelters are situated, is the province with
422 the largest Hg emissions in China; Shandong and Henan provinces are also large Hg emission areas,
423 emitting about 30-40 ton yr⁻¹ (Fu et al., 2012) in part due to a large lead smelter (Wang et al, 2014),
424 and biomass burning (Huang et al., 2011).

425 The probable source areas of PBM identified by PSCF were similar to those for TGM, indicating
426 that both Chinese and inland Korean sources enhanced PBM concentrations, with the exception of
427 metropolitan (Seoul) and industrial (Incheon) areas located in northwestern South Korea which
428 emerged as more prominent source areas for PBM than for TGM (Fig. 7). Only Korean sources
429 including metropolitan (Seoul) and the industrial areas in southern Korea were identified as probable

430 source areas for GOM (Fig. 7); regional transport of GOM from China was not important. The Yellow
431 Sea between China and Korea was also associated with high PSCF values, possibly indicating the
432 shipping ports located on the western coast of Korea as important source areas. However, it should be
433 noted that it might be a trailing effect derived by relatively short sampling duration. A trailing effect is
434 often observed, especially with a limited number of measurements or short sampling period, since
435 PSCF evenly distributes weight along the path of trajectories so that PSCF results often identify areas
436 upwind and downwind of real sources as a source area (Han et al., 2007). However, it should be also
437 noted that the marine boundary layer provides good conditions for active Hg oxidation reactions due
438 to an abundance of oxidants (Auzmendi-Murua et al., 2014); therefore, the possibility of areas over
439 the ocean being a GOM source should not be excluded.

440 **It should be noted that different temporal resolutions for trajectories (hourly) and concentrations**
441 **(every 12hr) were used for GOM and PBM. Since trajectory directions can significantly change over**
442 **the course of 12hrs there is a possibility that some source areas could be misidentified, especially for**
443 **more distant regional sources. However, upon investigation it was determined that over the 12 hr**
444 **sampling periods the trajectories did not diverge significantly at this sampling site for most sampling**
445 **periods.**

446

447 **3.2.3 Source attribution based on cluster analysis**

448 In an effort to quantify the contribution of national and foreign sources to the measured Hg
449 concentrations the back trajectories were grouped into five clusters using the trajectory cluster
450 analysis feature of HYSPLIT. Among the five clusters, clusters 1 and 5 represent trajectories
451 originating from outside (South) Korea whereas the trajectories grouped in the cluster 4 originated
452 and passed through the (South) Korean peninsula (Fig. 8). Clusters 2 and 3 contain trajectories from
453 China and the Korean peninsula, but cluster 2 was more associated with Liaoning province and North
454 Korea while cluster 3 originated more from Shandong and Henan provinces. Clusters 1 through 5
455 contributed 12%, 31%, 26%, 20%, and 11% of the total time, respectively, and the associated
456 concentrations with each cluster are shown in Table 4. Concentration ranges of three Hg species for

457 each cluster were shown as the box-and-whisker plots in the supplementary file (Fig. 5S). When
 458 considering that cluster 4 is associated with the local transport from inland Korea and the cluster 1 and
 459 5 are associated with the regional transport from outside of (South) Korea, the maximum and 75th
 460 percentile values as well as the arithmetic average are higher in cluster 4 for GOM and PBM than
 461 those in the clusters 1 and 5 (Fig. 5S).

462 The TGM concentration was the highest for cluster 5; however, GOM and PBM concentrations had
 463 the lowest averages for this cluster. Cluster 5 contains the back-trajectories originating from Mongolia
 464 and Russia and passing through northeastern China before arriving at the sampling site, which
 465 suggests regional transport was important for this cluster (Fig. 8). Average CO concentrations were
 466 pretty similar for all clusters, but it was the second highest for cluster 5 (cluster 2 was highest). The
 467 highest total average GOM and PBM concentrations were associated with cluster 4 which includes
 468 trajectories distributed over the Korean peninsula, suggesting that Korean sources were responsible
 469 for the enhanced GOM and PBM concentrations. For cluster 4, the highest Pearson correlation
 470 coefficient between GOM and PBM concentrations ($r=0.721$) was observed, indicating that both Hg
 471 species were emitted from similar sources. For other clusters, there were no statistically significant
 472 correlations between GOM and PBM except for cluster 2 ($r=0.209$, $p\text{-value}<0.001$). In addition, both
 473 average NO₂ concentration (19.4 ± 14.9 ppb) and the correlation coefficient between NO₂ and TGM
 474 ($r= 0.688$) were the highest for cluster 4, supporting the finding of impact from Korean sources.

475 In order to consider both Hg concentration and the fraction of time for each cluster, the following
 476 equation was used to quantify the effect of Korean and out-of- Korean sources to the Hg concentration
 477 at the receptor site.

$$478 \quad \text{source contribution of cluster, } i = \frac{\left(\frac{N_i}{N_{total}}\right) \times C_j}{\sum_{i=1}^n \left\{ \left(\frac{N_i}{N_{total}}\right) \times C_j \right\}} \quad (\text{Eq.6})$$

479 where (N_i/N_{total}) indicates the percentage of time associated with the cluster, i , i is the cluster number,
 480 n is the number of clusters (equal to five in this study), and C_j indicates the average Hg concentration
 481 associated with the cluster, i . Compared to the other clusters, the source contributions of clusters 1 and
 482 5, which represent regional transport, were relatively low for all Hg species (Table 4). Cluster 4

483 contributed more significantly, especially for GOM and PBM, indicating the importance of Korean
484 sources. The source contribution of cluster 2 was the highest for PBM compared to other Hg species,
485 suggesting that North Korean sources were an important contributor to the high PBM concentrations
486 measured, likely due to coal and biomass burning in North Korea (Kim et al., 2013; NI, 2001; NI,
487 2003).

488 In order to quantify the contribution of Korean vs. out-of-Korean sources (note that “Korean”
489 means “South Korean” throughout the manuscript), the source contributions of the clusters were used.
490 Clusters 1 and 5 were used to represent the effect of sources outside of Korea and the cluster 4 was
491 used to indicate the effect of sources in Korea. Since clusters 2 and 3 contain mixed trajectories from
492 Korea and out-of-Korea their contribution was divided evenly between in and out of Korea. The
493 results indicate that the sources in Korea and outside Korea contributed about 50% each to the
494 concentration variation of TGM measured at the sample site during the sampling period while the
495 Korean sources affected GOM and PBM more significantly, accounting for approximately 52.3% and
496 53.4%, respectively (Table 4). These results augment the CPF and PSCF results which only use
497 concentrations that are in the top 25th percentile. While CPF and PSCF found that for high
498 concentration events Korean sources were most important for GOM while for TGM and PBM
499 regional transport from China and North Korea were also important, the cluster based approach
500 suggests that for all 3 species Korean and out-of-Korean sources contributed approximately 50% each
501 to the concentration variations seen by the site. When the geometric mean concentrations were used
502 for each cluster a similar result was obtained for relative contributions as the results using arithmetic
503 mean concentrations.

504 It should be noted that errors always exist in calculating trajectories, causing uncertainties in all
505 trajectory-based approaches. Trajectory errors vary considerably from case to case; Stohl (1998)
506 suggested uncertainties might be 20% of the distance travelled by trajectories while Draxler (1996)
507 found that the final error was about 10% of the travel distance.

508

509 **4. Conclusion and Implications**

510 This study was initiated to identify the sources affecting speciated mercury concentrations
511 measured on an island located between mainland Korea and Eastern China. Various tools were used
512 to locate and quantify the sources, including correlations with other pollutants, CPF, and the back-
513 trajectory based analysis (PSCF and cluster analysis). The results consistently show that Korean
514 sources are most important for GOM while for other Hg species (TGM and PBM) regional transport
515 from China and North Korea were also important. Existing methods including PSCF and CPF are able
516 to locate the source direction and areas, but do not consider the frequency of the wind directions
517 which can affect the long-term concentrations at the receptor site. For example, if the Hg
518 concentration is high with easterly winds both CPF and PSCF identify the eastern areas as important
519 source areas even if, in fact, winds are rarely blowing from east. In this work, it is true that sources
520 located in the eastern direction from the sampling site are likely to be important for enhancing Hg
521 concentrations, but based only on CPF and PSCF results it cannot be said that their contribution to the
522 concentration variations at the site is also high.

523 Do address this problem a new approach that considers both the cluster frequency and the Hg
524 concentration associated with each cluster was used to quantify the source contribution at the
525 sampling site. **On average, contributions from out-of-Korean sources were similar to Korean sources
526 for TGM whereas Korean sources contributed slightly more to the concentration variations of GOM
527 and PBM compared to the out-of-Korean sources. However, in general, conclusions using this
528 approach are more uncertain when the concentration ranges are similar between clusters. Additional
529 work is needed with this approach to determine if a different statistic (other than mean) would provide
530 better results when there are not distinct concentration differences between clusters. In addition,
531 uncertainties exist in the source attribution approach based on cluster analysis because the trajectories
532 inevitably overlap between different clusters since the cluster analysis accounts for both variations in
533 transport speed and direction simultaneously. Nevertheless, this new approach can augment existing
534 methods including CPF and PSCF to help identify source contributions to the concentration variations
535 at the sampling site.**

536 The ratio of GOM/PBM proved to be a useful tool for identifying the relative significance of local

537 sources vs. regional transport. The GOM/PBM ratio decreased as the effect of regional transport
538 increased and vice versa since GOM has a shorter atmospheric residence time than PBM. The K_p
539 calculated using the reciprocal of the GOM/PBM ratio was negatively correlated with atmospheric
540 temperature and positively correlated with relative humidity, suggesting that the secondary formation
541 of PBM was an important source of atmospheric PBM concentration at low temperature and high
542 relative humidity. This result also suggests that the secondary formation of PBM becomes more
543 favored when the air undergoes regional transport rather than local transport.

544

545 **Acknowledgements**

546 This work was funded by the National Research Foundation of Korea (NRF) grant funded by the
547 Korea government (MSIP) (No. 2015R1A2A2A03008301) and the Korea Ministry of Environment
548 (MOE) as “the Environmental Health Action Program”. This research was also supported by 2014
549 Research Grant from Kangwon National University (No. C1011758-01-01).

550

551 **Author Contributions**

552 The work presented here was carried out in collaboration between all authors. Gang S. Lee analyzed
553 data and wrote the paper. Pyung R. Kim performed the experiments and interpreted the results. Young
554 J. Han defined the research theme, interpreted the results, and wrote the paper. Yong S. Seo, Seung.
555 M. Yi, and Thomas M. Holsen also interpreted the results and approved the final paper.

556

557 **Conflicts of Interest**

558 The authors declare no conflict of interest.

559

560 **Reference**

561 AMAP/UNEP: Technical Background Report on the Global Anthropogenic Mercury Assessment;
562 Arctic Monitoring and Assessment Programme/UNEP Chemicals Branch, p. 159., 2008.

563

564 Amato, F. and Hopke, P.K.: Source apportionment of the ambient PM_{2.5} across St. Louis using
565 constrained positive matrix factorization, *Atmos. Environ.*, 329-337, 2012.
566

567 Amos, H. M., Jacob, D. J., Holmes, C. D., Fisher, J. A., Wang, Q., Yantosca, R. M., Corbitt, E. S.,
568 Galarneau, E., Rutter, A. P., Gustin, M. S., Steffen, A., Schauer, J. J., Graydon, J. A., St Louis, V. L.,
569 Talbot, R. W., Edgerton, E. S., Zhang, Y., and Sunderland, E. M.: Gas-particle partitioning of
570 atmospheric Hg(II) and its effect on global mercury deposition, *Atmos. Chem. Phys.*, 12, 591–603,
571 2012.
572

573 Ariya, P.A.: Atmospheric science: mid-latitude mercury loss, *Nature Geoscience*, 4, 14-15, 2011.
574

575 Auzmendi-Murua, I., Castillo, A. and Bozzelli J.W.: Mercury Oxidation via Chlorine, Bromine, and
576 Iodine under atmospheric conditions: Thermochemistry and Kinetics, *J. Phy. Chem.*, 118, 2959-2975,
577 2014.
578

579 Baya, A.P. and Van Heyst, B.: Assessing the trends and effects of environmental parameters on the
580 behaviour of mercury in the lower atmosphere over cropped land over four season, *Atmos. Chem.*
581 *Phys.*, 10, 8617-8628, doi:10.5194/acp-10-8617-2010, 2010.
582

583 Cheng, L., Zhang, L., and Blanchard, P.: Regression modeling of gas-particle partitioning of
584 atmospheric oxidized mercury from temperature data, *J. of Geophy. Res. Atmos.*, 119(20), 11864-
585 11876, 2014.
586

587 Cheng, I., Zhang, L., Mao, H., Blanchard, P., Tordon, R. and John, D.: Seasonal and diurnal patterns
588 of speciated atmospheric mercury at a coastal-rural and coastal-urban site, *Atmos. Environ.*, 82, 193–
589 205, 2014.
590

591 Choi, H. D., Holsen, T. M. and Hopke, P. K.: Atmospheric mercury in the Adirondacks:
592 concentrations and sources, *Environ. Sci. Technol.*, 42, 5644-5653, 2008.
593
594 Draxler, R.R.: Trajectory optimization for balloon flight planning, *Weather and Forecasting*, 11, 111-
595 1114, 1996.
596
597 Draxler, R.R., Stunder, B., Rolph, G., Stein, A. and Taylor, A.: HYSPLIT_4 User's Guide. Silver
598 Spring, Maryland, USA: NOAA Air Resour. Lab., Available at
599 http://www.arl.noaa.gov/documents/reports/hysplit_user_guide.pdf, 2014.
600
601 Driscoll, C.T., Han, Y.J., Chen, C.Y., Evers, D.C., Lambert, K.F., Holsen, T.M., Kamman, N.C. and
602 Munson, R.K.: Mercury contamination in forest and freshwater ecosystems in the Northeastern United
603 States, *Bioscience*, 57, 17–28, 2007.
604
605 Edgerton, E.S., personal communication.
606
607 Fang, G.C., Zhang, L. and Huang, C.S.: Measurement of size-fractionated concentration and bulk dry
608 deposition of atmospheric particulate bound mercury, *Atmos. Environ.*, 61, 371–377, 2012.
609
610 Feng, X., Lu, J.Y., Conrad, D.G., Hao, Y., Banic, C.M. and Schroeder, W.H.: Analysis of inorganic
611 mercury species associated with airborne particulate matter/aerosols: method development, *Anal.*
612 *Bioanal. Chem.*, 380, 683-689, 2004
613
614 Finley, B.D., Jaffe, D.A., Call, K., Lyman, S., Gustin, M.S., Peterson, C., Miller, M. and Lyman, T.:
615 Development, testing, and deployment of an air sampling manifold for spiking elemental and oxidized
616 mercury during the Reno atmospheric mercury intercomparison experiment (RAMIX). *Environ. Sci.*
617 *Technol.* 47(13), 7277-7284, 2013.

618
619
620
621
622
623
624
625
626
627
628
629
630
631
632
633
634
635
636
637
638
639
640
641
642
643
644

Fu, X., Feng, X., Qiu, G., Shang, L. and Zhang, H.: Speciated atmospheric mercury and its potential source in Guiyang, China, *Atmos. Environ.*, 45, 4205–4212, 2011.

Galindo, N., Yubero, E., Nicolás, J.F., Crespo, J., Pastor, C., Carratalá, A., and Santacatalina, M.: Water-soluble ions measured in fine particulate matter next to cement works, *Atmos. Environ.*, 45, 2043-2049, 2011.

Gratz, L.E., Keeler, G.J., Marsik, F.J., Barres, J.A., Dvonch, T.: Atmospheric transport of speciated mercury across southern Lake Michigan: Influence from emission sources in the Chicago/Gary urban area, *Sci. Total Environ.*, 448, 84-95, 2013.

Gustin, M.S., Huang, J., Miller, M.B., Peterson, C., Jaffe, D.A., Ambrose, J., Finley, B.D., Lyman, S.N., Call, K., Talbot, R., Feddersen, D., Mao, H. and Lindberg, S.E.: Do we understand what the mercury speciation instruments are actually measuring? Results of RAMIX. *Environ. Sci. Technol.* 47(13), 7295-7306, 2013.

Gustin, M.S., Amos, H.M., Huang, J., Miller, M.B., and Heidecorn, K.; Measuring and modeling mercury in the atmosphere: a critical review, *Atmos. Chem. Phys.*, 15, 5697-5713, 2015.

Han, Y.J., Holsen, T.M. and Hopke, P.K.: Estimation of source location of total gaseous mercury measured in New York State using trajectory-based models, *Atmos. Environ.*, 41, 6033–6047, 2007.

Han, Y. J., Kim, J. E., Kim, P. R., Kim, W. J., Yi, S. M., Seo, Y. S. and Kim, S. H.: General trends of Atmospheric mercury concentrations in urban and rural areas in Korea and characteristics of high-concentration events, *Atmos. Environ.*, 94, 754-764, 2014.

645 Hedgecock, I. M. and Pirrone, N.: Chasing quicksilver: Modeling the atmospheric lifetime of Hg⁰ (g)
646 in the marine boundary layer at various latitudes, *Environ. Sci. Technol.*, 38(1), 69-76, 2004.
647

648 Huang, J., Choi, H.D., Hopke, P.K. and Holsen, T.M.: Ambient mercury sources in Rochester, NY :
649 Results from principal components analysis (PCA) of mercury monitoring network data. *Environ. Sci.*
650 *Technol.*, 44, 8441-8445, 2010.
651

652 Huang, X., Li, M., Friedli, H. R., Song, Y., Chang, D. and Zhu, L.: Mercury Emissions from Biomass
653 Burning in China. *Environ. Sci. Technol.*, 45, 9442-9448, 2011.

654 Huang, J. and Gustin, M.S.: Evidence for a free troposphere source of mercury in wet deposition in
655 the Western United States, *Environ. Sci. Technol.*, 46(12), 6621-6629, 2012.
656

657 Huang, J., Miller, M.B., Weiss-Penzias, P. and Gustin, M.S.: Comparison of gaseous oxidized Hg
658 measured by KCl-coated denuders, and nylon and cation exchange membranes. *Environ. Sci. Technol.*,
659 47(13), 7307-7316, 2013.
660

661 IEA, International Energy Agency :
662 http://www.iea.org/stats/countryresults.asp.COUNTRY_CODE=KP&Submit=Submit: 2012.
663

664 Jaffe, D.A., Lyman, S., Amos, H.M., Gustin, M.S., Huang, J., Selin, N.E., Levin, L., Sschure, A.T.,
665 Mason, R.P., Talbot, R., Rutter, A., Finley, B., Jaeglé, L., Shah, V., McClure, C., Ambrose, J., Gratz,
666 L., Lindberg, S., Weiss-Penzias, P., Sheu, G.R., Feddersen, D.D., Horvat, M., Dastoor, A., Hynes, A.J.,
667 Mao, H., Sonke, J.E., Slemr, F., Fisher, J.A., Ebinghaus, R., Zhang, Y. and Edwards, G.: Progress on
668 understanding atmospheric mercury hampered by uncertain measurements, *Environ. Sci. Technol.*, 48,
669 7204-7206, 2014.
670

671 Kelly, C., Toro, R., Di Martino, A., Cox, C.L., Bellec, P., Castellanos, F.X., and Milham, M.P.: A

672 convergent functional architecture of the insula emerges across imaging modalities, *Neuroimage*, 61,
673 1129-1142, 2012.

674

675 Kim, J.H., Park, J.M., Lee, S.B., Pudasainee, D. and Seo, Y.C.: Anthropogenic mercury emission
676 inventory with emission factors and total emission in Korea, *Atmos. Environ.*, 44, 2714-2721, 2010.

677

678 Kim, M., Deshpande, S.R, Crist, K.C.: Source apportionment of fine particulate matter (PM_{2.5}) at a
679 rural Ohio River Valley site, *Atmos. Environ.*, 41, 9231-9243, 2007.

680

681 Kim, I.S., Lee, J.Y., and Kim, Y.P.: Impact of polycyclic aromatic hydrocarbon (PAH) emissions from
682 North Korea to the air quality in the Seoul Metropolitan Area, South Korea, *Atmos. Environ.*, 70, 159-
683 165, 2013.

684

685 Kim, P. R., Han, Y.J., Holsen, T.M. and Yi, S.M.: Atmospheric particulate mercury: Concentrations
686 and size distributions, *Atmos. Environ.*, 61, 94-102, 2012.

687

688 Kim, S.H., Han, Y.J., Holsen, T.M. and Yi, S.M.: Characteristics of atmospheric speciated mercury
689 concentrations (TGM, Hg(II), and Hg(p)) in Seoul, Korea, *Atmos. Environ.*, 43, 3267-3274, 2009.

690

691 Lan, X., Talbot, R., Castro, M., Perry, K. and Luke, W.: Seasonal and Diurnal Variations of
692 Atmospheric Mercury across the US Determined from AMNet Monitoring Data, *Atmos. Chem. Phys.*,
693 12, 10569–10582, 2012.

694

695 Landis, M.S. and Keeler, G.J.: Atmospheric mercury deposition to Lake Michigan during the Lake
696 Michigan mass balance study, *Environ. Sci. Technol.*, 36, 4518-4524, 2002

697

698 Lee, G.S., Kim, P.R., Han, Y.J., Holsen, T.M., and Lee, S.H.: Tracing sources of total gaseous mercury

699 to Yongheung Island off the coast of Korea, *Atmosphere*, 5, 273-291, 2014.

700

701 Lin, C. J. and Pehkonen, S. O.: The chemistry of atmospheric mercury: a review, *Atmos. Environ.*,

702 33(13), 20674-2079, 1999.

703

704 Lyman, S.N. and Gustin, M.S.: Determinants of atmospheric mercury concentrations in Reno, Nevada,

705 USA. *Sci. Total. Environ.*, 408, 431-438, 2009.

706

707 Lyman, S.N.; Jaffe, D.A. and Gustin, M.S.: Release of mercury halides from KCl denuders in the

708 presence of ozone. *Atmos. Chem. Phys.* 10(17), 8197-8204, 2010.

709

710 Lynam, M. M. and Keeler, G. J.: Automated speciated mercury measurements in Michigan, *Environ.*

711 *Sci. Technol.*, 39, 9253-9562, 2005.

712

713 Liu, B., Keeler, G.J., Timothy Dvonch, J., Barres, J.A., Lynam, M.M., Marsik, F.J. and Morgan, J.T.:

714 Urban-rural differences in atmospheric mercury speciation, *Atmos. Environ.*, 44, 2013-2023, 2010.

715

716 Lu, W., Zhu, Z.Y. and Liu, W.P.: Salt water intrusion numerical simulation on application based on

717 FEFLOW, *Ground Water*, 32, 19–21, 2010.

718

719 McClure, C.D., Jaffe, D.A. and Edgerton, E.S.: Evaluation of the KCl denuder method for gaseous

720 oxidized mercury using HgBr₂ at an In-Service AMNet site, *Environ. Sci. Technol.*, 48, 11437-11444,

721 2014.

722

723 Malcolm, E.G. and Keeler, G.J.: Evidence for a sampling artifact for particulate-phase mercury in the

724 marine atmosphere, *Atmos. Environ.* 41(16), 3352-3359, 2007.

725

726 Mao, H., Talbot, R., Hegarty, J., and Koermer, J.: Speciated mercury at marine, coastal, and inland
727 sites in New England Part 2: Relationships with atmospheric physical parameters, *Atmos. Chem.*
728 *Phys.*, 12, 4181-4206, 2012.

729

730 Mason, R.P., Morel, F.M.M. and Hemond, H.F.: The role of microorganisms in elemental mercury
731 formation in natural water, *Water Air Soil Poll*, 80, 775-787, 1995.

732

733 Mason, R.P. and Sullivan, K.A.: Mercury in Lake Michigan, *Environ. Sci. Technol.*, 31, 942-947,
734 1997.

735

736 Mergler, D., Anderson, H.A., Chan, L.H.M., Mahaffey, K.R., Murray, M., and Sakamoto, M.:
737 Methylmercury exposure and health effects in humans: a worldwide concern, *Ambio* 36:3-11, 2007.

738

739 NI, Nautilus Institute for Security and Sustainable Development: Rural energy survey in U nhari
740 Village, the Democratic People's Republic of Korea (DPRK): Methods, results, and implications,
741 Berkely, California, USA, 2001.

742

743 NI, Nautilus Institute for Security and Sustainable Development: The DPRK Energy Sector:
744 Estimated Year 2000 Energy Balance and Suggested Approaches to Sectoral Redevelopment,
745 Berkeley, California, USA, 2003

746

747 Obrist, D., Johnson, D. W., Lindberg, S. E., Luo, Y., Hararuk, O., Bracho, R., Battles, J. J., Dail, D. B.,
748 Edmonds, R. L., Monson, R. K., Ollinger, S. V., Pallardy, S. G., Pregitzer, K. S. and Todd D. E.:
749 Mercury Distribution Across 14 U.S. Forests. Part I: Spatial Patterns of Concentrations in Biomass,
750 Litter, and Soils, *Environ. Sci. Technol.*, 45(9), 3974-3981, 2011.

751

752 Pirrone, N., Aas, W., Cinnirella, S., Ebinghaus, R., Hedgecock, I. M., Pacyna, J., Sprovieri, F. and

753 Sunderland, E. M.: Toward the next generation of air quality monitoring: Mercury, *Atmos. Environ.*,
754 80, 599-611, 2013.

755

756 Pirrone, N., Keeler, G. J. and Nriagu, J. O.: Regional differences in worldwide emissions of mercury
757 to the atmosphere, *Atmos. Environ.*, 30, 2981–2987, 1996.

758

759 Polissar, A.V., Hopke, P.K. and Harris, J.M.: Source regions for atmospheric aerosol measured at
760 Barrow, Alaska, *Environ. Sci. Technol.*, 35, 4214–4226, 2001.

761

762 Polissar, A.V., Hopke, P.K. and Poirot, R.L.: Atmospheric aerosol over Vermont: Chemical
763 composition and sources, *Environ. Sci. Technol.*, 35, 4604–4621, 2001.

764

765 Rutter, A.P. and Schauer, J.J.: The effect of temperature on the gas-particle partitioning of reactive
766 mercury in atmospheric aerosols, *Atmos. Environ.*, 41, 8647-8657, 2007a

767

768 Rutter, A.P. and Schauer, J.J.: The impact of aerosol composition on the particle to gas partitioning of
769 reactive mercury, *Environ. Sci. Technol.*, 41(11), 3934-3939, 2007b

770

771 Seinfeld, J.H. and Pandis, S. N.: *Atmospheric chemistry and physics: From air pollution to climate*
772 *change*, second ed. John Wiley & Sons, Inc., Hoboken, New Jersey, USA, 2006.

773

774 Stohl, A.: Computation, accuracy and applications of trajectories- A review and bibliography, *Atmos.*
775 *Environ.*, 32(6), 947-966, 1998.

776

777 Subir, M., Ariya, P. A., and Dastoor, A. P.: A review of uncertainties in atmospheric modeling of
778 mercury chemistry I. Uncertainties in existing kinetic parameters–Fundamental limitations and the
779 importance of heterogeneous chemistry, *Atmos. Environ.*, 45(32), 5664-5676, 2011.

780

781 Subir, M., Ariya, P. A., and Dastoor, A. P.: A review of the sources of uncertainties in atmospheric
782 mercury modeling II. Mercury surface and heterogeneous chemistry—A missing link, *Atmos. Environ.*,
783 46, 1-10, 2012.

784

785 Talbot, R., Mao, H., Feddersen, D., Smith, M., Kim, S.Y., Sive, B., Haase, K., Ambrose, J., Zhou, Y.
786 and Russo, R.: Comparison of particulate mercury measured with manual and automated methods,
787 *Atmosphere*, 2, 1-20, 2011.

788

789 Temme, C., Einax, Jr., W., Ebinghaus, R., and Schroeder, W.H.: Measurements of atmospheric
790 mercury species at a coastal site in the Antarctic and over the South Atlantic Ocean during polar
791 summer, *Environ. Sci. Technol.*, 37, 22-31, 2002

792

793 Timonen, H., Ambrose, J.L., Jaffe, D.A.: Oxidation of elemental Hg in anthropogenic and marine
794 airmasses, *Atmos. Chem. Phys.*, 13, 2827-2836, 2013.

795

796 U.S. EPA,: Mercury Study Report to Congress. Office of Air Quality Planning and Standards and
797 Office of Research and Development, EPA-452/R-97-005, 1997.

798

799 UNEP.: The Global Atmospheric Mercury Assessment; UNEP Chemicals Branch: Geneva,
800 Switzerland, 2013.

801

802 Wan, Q., Feng, X.B., Julia, L., Zheng, W., Song, X.J., Han, S.J., and Xu, H.: Atmospheric mercury in
803 Changbai Mountain area, northeastern China – Part 1: The seasonal distribution pattern of total
804 gaseous mercury and its potential sources, *Environ. Res.*, 109, 201-206, 2009a

805

806 Wan, Q., Feng, X.B., Julia, L., Zheng, W., Song, X.J., Han, S.J., and Xu, H.: Atmospheric mercury in

807 Changbai Mountain area, northeastern China II. The distribution of reactive gaseous mercury and
808 particulate mercury and mercury deposition fluxes, *Environ. Res.*, 109, 721-727, 2009b
809

810 Wang, L., Wang, S., Zhang, L., Wang, Y., Zhang, Y., Nielsen, C., McElroy, B. M. and Hao, J.: Source
811 apportionment of atmospheric mercury pollution in China using the GEOS-Chem model, *Environ.*
812 *Poll.*, 190, 166-175, 2014.
813

814 Wang, S., Holsen, T.M., Huang, J. and Han, Y.J.: Evaluation of various methods to measure
815 particulate bound mercury and associated artifacts, *Atmos. Chem. Phys. Discuss.* 13, 8585-8614, 2013.
816

817 Weiss-Penzias, P., Jaffe, D.A., McClintick, A., Prestbo, E.M. and Landis, M.S.: Gaseous elemental
818 mercury in the marine boundary layer: evidence for rapid removal in anthropogenic pollution,
819 *Environ. Sci. Technol.*, 37, 3755-3763, 2003.
820

821 Weiss-Penzias, P., Jaffe, D.A., Swartzendruber, P., Dennison, J.B., Chand, D., Hafner, W. and Prestbo,
822 E.: Observations of Asian air pollution in the free troposphere at Mount Bachelor Observatory during
823 the spring of 2004, *J. Geophys. Res.*, 111 (D10304), 1-15, 2006.
824

825 Weiss-Penzias, P., Gustine, M.S., Lyman, S.: Observations of speciated atmospheric mercury at three
826 sites in Nevada, USA: Evidence for a free tropospheric source of reactive gaseous mercury, *J. of*
827 *Geophys. Res.*, 114, D14302, doi:10.1029/2008JD011607, 2009
828

829 Xiu, G.L., Jin, Q.X., Zhang, D.N., Shi, S.Y., Huang, X.J., Zhang, W.Y., Bao, L., Gao, P.T. and Chen,
830 B.: Characterization of size-fractionated Particulate Mercury in Shanghai Ambient Air. *Atmos,*
831 *Environ.*, 39, 419-427, 2005.
832

833 Xiu, G.L., Cai, J., Zhang, W.Y., Zhang, D.N., Bueller, A., Lee, S.C., Shen, Y., Xu, L.H., Huang, X.J.

834 and Zhang, P.: Speciated Mercury In size Fractionated Particles in Shanghai Ambient Air, *Atmos.*
835 *Environ.*, 43, 3145–3154, 2009.

836

837 Xu, L.L., Chen, J.S., Yang, L.M., Niu, Z.C., Tong, L., Yin, L.Q., and Chen, Y.T.: Characteristics and
838 sources of atmospheric mercury speciation in a coastal city, Xiamen, China, *Chemosphere*, 119, 530-
839 539, 2015.

840

841 You, C.H., Kim, B.G., Jo, E.M., Kim, G.Y., Yu, B.C., Hong, M.G., Kim, D.S., and Hong, Y.S.: The
842 relationship between the fish consumption and blood total/methyl-mercury concentration of coastal
843 area in Korea, *NeuroToxicology*, 33, 676-682, 2012.

844

845 Zhang, H., Feng, X., Larseen, T., Qiu, G., and Vogt, R.D.: In inland China, rice, rather than fish, is the
846 major pathway for methylmercury exposure, *Environmental Health Perspectives*, 118, 1183-1188,
847 2010.

848

849 Zhang, L., Gong, S., Padro, J. and Barrie, L.: A size-segregated particle dry deposition scheme for and
850 atmospheric aerosol module, *Atmos. Environ.*, 35, 549–560, 2001.

851

852 Zhang, H., Fu, X.W., Lin, C.-J., Wang, X., and Feng, X.B.: Observation and analysis of speciated
853 atmospheric mercury in Shangri-La, Tibetan Plateau, China, *Atmos. Chem. Phys.*, 15, 653-665, 2015.

854

855 **Table list**

856 Table 1 Summarized concentrations of speciated Hg and other typical pollutants for each sampling
857 period.

858

859 Table 2. Comparisons of measured Hg concentrations with those reported in other studies.

860

861 Table 3. Correlation coefficients and p-values (in parenthesis) for speciated Hg with other pollutants
862 for the whole sampling period. Correlation coefficients with an asterisk indicate a statistically
863 significant relationship at $\alpha = 0.05$.

864

865 Table 4. Estimated contribution of Korean and out-of-Korean sources on variations of speciated Hg
866 concentration. *: TGM is shown in ng m^{-3} while for both GOM and PBM the units are pg m^{-3} .

867

868

869

870

871

872

873

874

875

876

877

878

879

880

881

882 **Figure list**

883 Figure 1. (a) The sampling site in Yongheung Island (the star mark). (b) Anthropogenic mercury
884 emission sources in Korea. Blue star indicates the sampling site, and the green circle indicates the area
885 where major Korean coal-fired power plants are located. (c) The enlarged image of the area near the
886 sampling site.

887

888 Figure 2. TGM, GOM, and PBM concentrations measured during the eight sampling periods. TGM
889 was measured every 5 minutes while GOM and PBM were measured during 12hrs except for the 2hr
890 measurements during May, 2014.

891

892 Figure 3. Box-and-whisker plot for the concentrations of TGM, GOM, and PBM during three
893 different periods. The red dash lines indicate the arithmetic mean.

894

895 Figure 4. The gas-particle partitioning coefficient, K_p , related to atmospheric temperature and relative
896 humidity (RH) (n=81)..

897

898 Figure 5. CPF plots for TGM using the top 25% (left upper panel) and the top 10% (right upper panel)
899 as a criterion, and for GOM (left bottom panel) and for PBM (right bottom panel). For both GOM and
900 PBM, the criterion of the top 25% concentration was used.

901

902 Figure 6. Frequency of wind direction with different GOM/PBM ratios. Southerly and easterly winds
903 prevailed for the samples with high GOM/PBM ratio whereas the percentage of westerly winds
904 increased as the GOM/PBM ratio decreased.

905

906 Figure 7. PSCF results for TGM (left), PBM (middle), and GOM (right) using the top 25% of
907 concentrations as criteria.

908

909 Figure 8. Back-trajectories for clusters 1 through 5. The left top panel indicates the mean back-
910 trajectory and contribution for each cluster.

Table 1 Summarized concentrations of speciated Hg and other typical pollutants for each sampling period

Sampling periods	TGM (ng m ⁻³)	GOM (pg m ⁻³)	PBM (pg m ⁻³)	SO ₂ (ppb)	NO ₂ (ppb)	CO (ppm)	O ₃ (ppb)	PM ₁₀ (μg m ⁻³)
1 st : 2013.01.17 ~ 01.23	3.5 ± 0.8	5.8 ± 8.8	17.0 ± 16.5	5.8 ± 4.2	26.7 ± 12.4	0.5 ± 0.2	21.7 ± 13.5	55.9 ± 38.5
2 nd : 2013.02.25 ~ 03.01	3.7 ± 0.9	13.2 ± 14.8	19.5 ± 19.6	7.3 ± 3.0	28.8 ± 19.1	0.7 ± 0.2	28.3 ± 14.7	83.6 ± 28.6
3 rd : 2013.04.08 ~ 04.13	2.1 ± 0.4	4.3 ± 5.6	15.6 ± 13.8	4.9 ± 1.7	8.6 ± 3.3	0.4 ± 0.1	46.8 ± 6.0	45.8 ± 21.4
4 th : 2013.05.20 ~ 05.25	2.8 ± 1.0	4.2 ± 5.9	6.7 ± 7.3	5.7 ± 2.5	17.2 ± 5.9	0.5 ± 0.1	36.2 ± 19.4	51.9 ± 21.6
5 th : 2013.08.19 ~ 08.24	2.3 ± 0.9	3.2 ± 3.0	5.4 ± 4.6	4.7 ± 1.6	10.2 ± 3.8	0.5 ± 0.1	40.9 ± 29.6	34.2 ± 13.7
6 th : 2014.03.17 ~ 03.21	2.6 ± 1.2	12.8 ± 15.7	7.3 ± 3.5	7.5 ± 0.1	32.9 ± 75.1	0.4 ± 0.2	39.0 ± 12.5	66.7 ± 44.4
7 th : 2014.05.26 ~ 05.31	2.8 ± 0.7	13.5 ± 9.0	9.8 ± 12.2	5.8 ± 2.3	12.4 ± 5.6	0.5 ± 0.1	85.5 ± 23.3	124.5 ± 44.9
8 th : 2014.08.19 ~ 08.23	2.4 ± 1.1	10.7 ± 3.7	6.3 ± 3.6	3.4 ± 1.2	8.7 ± 6.0	0.4 ± 0.1	38.7 ± 16.5	32.0 ± 22.3
Average	2.8 ± 1.1	8.3 ± 9.7	10.9 ± 11.2	5.6 ± 5.0	18.2 ± 28.7	0.5 ± 0.2	42.1 ± 25.8	61.9 ± 42.8

Table 2. Comparisons of measured Hg concentrations with those reported in other studies.

Country	Site	Remarks	Year	TGM (ng m ⁻³)	GOM (pg m ⁻³)	PBM (pg m ⁻³)	Reference
Korea	Seoul	Urban	2005-2006	3.22 ± 2.10	27.2 ± 19.3	23.9 ± 19.6	Kim et al., 2009
	Seoul	Urban	2006-2009	3.72 ± 2.96	11.3 ± 9.5	13.4 ± 12.0	Han et al., 2014
	Chuncheon	Rural	2006-2009	2.12 ± 1.47	2.7 ± 2.7	3.7 ± 5.7	Han et al., 2014
	Yongheung	Island	2013-2014	2.8 ± 1.1	9.8 ± 9.9	10.6 ± 12.0	This study
China	Guiyang	Urban	2009	9.7 ± 10.2	35.7 ± 43.9	368.0 ± 676.0	Fu et al., 2011
	Xiamen	Suburban	2012-2013	3.5	61.05	174.41	Xu et al., 2015
	Mt. Changbai	Remote	2005-2006	3.58 ± 1.78	65 ± 84	77 ± 136	Wan et al., 2009a,b
USA	Chicago	Urban	2007	2.5 ± 1.5	17 ± 87	9 ± 20	Gratz et al., 2013
	Reno, Nevada	Suburban	2007-2009	2.0 ± 0.7	18 ± 22	7 ± 7	Lyman and Gustin, 2009
	Rochester, NY	Urban	2008-2009	1.49	4.08	6.57	Huang et al., 2010
Canada	Nova Scotia	Urban	2010-2011	1.67 ± 1.01	2.07 ± 3.35	2.32 ± 3.09	Cheng et al., 2014
	Ontario	Rural	2006-2007	1.17	15.10	16.40	Baya and Van Heyst, 2010

Table 3. Correlation coefficients and p-values (in parenthesis) for speciated Hg with other pollutants for the whole sampling period. Correlation coefficients with an asterisk indicate a statistically significant relationship at $\alpha = 0.05$.

	TGM	GOM	SO₂	NO₂	CO	O₃	PM₁₀
TGM	-	-0.132 (0.233)	0.115* (0.001)	0.063 (0.074)	0.571* (<0.001)	-0.055 (0.115)	0.401** (<0.001)
GOM	-0.132 (0.233)	-	0.025 (0.822)	0.022 (0.846)	-0.149 (0.180)	0.143 (0.197)	0.128 (0.248)
PBM	0.235* (0.030)	0.021 (0.855)	-0.006 (0.954)	0.008 (0.941)	0.215* (0.048)	0.029 (0.794)	0.139 (0.206)

Table 4. Estimated contribution of Korean and out-of-Korean sources on variations of speciated Hg concentration.

*: TGM is shown in ng m^{-3} while for both GOM and PBM the units are pg m^{-3} .

Cluster	Cluster frequency (%)	Average concentration *			Source contribution (%)			Korean (%)			Out-of-Korean (%)		
		TGM	GOM	PBM	TGM	GOM	PBM	TGM	GOM	PBM	TGM	GOM	PBM
1	12	2.2	6.9	7.7	9.6	10.5	8.6				9.6	10.5	8.6
2	31	2.8	8.3	12.6	31.5	32.5	36.5	15.7	16.3	18.2	15.7	16.3	18.2
3	26	2.9	8.1	10.0	27.3	26.6	24.3	13.7	13.3	12.1	13.7	13.3	12.1
4	20	2.6	9.0	12.3	18.9	22.8	23.0	18.9	22.8	23.0			
5	11	3.2	5.5	7.4	12.8	7.6	7.6				12.8	7.6	7.6
Korean								48.3	52.3	53.4			
Out-of-Korean											51.7	47.7	46.6

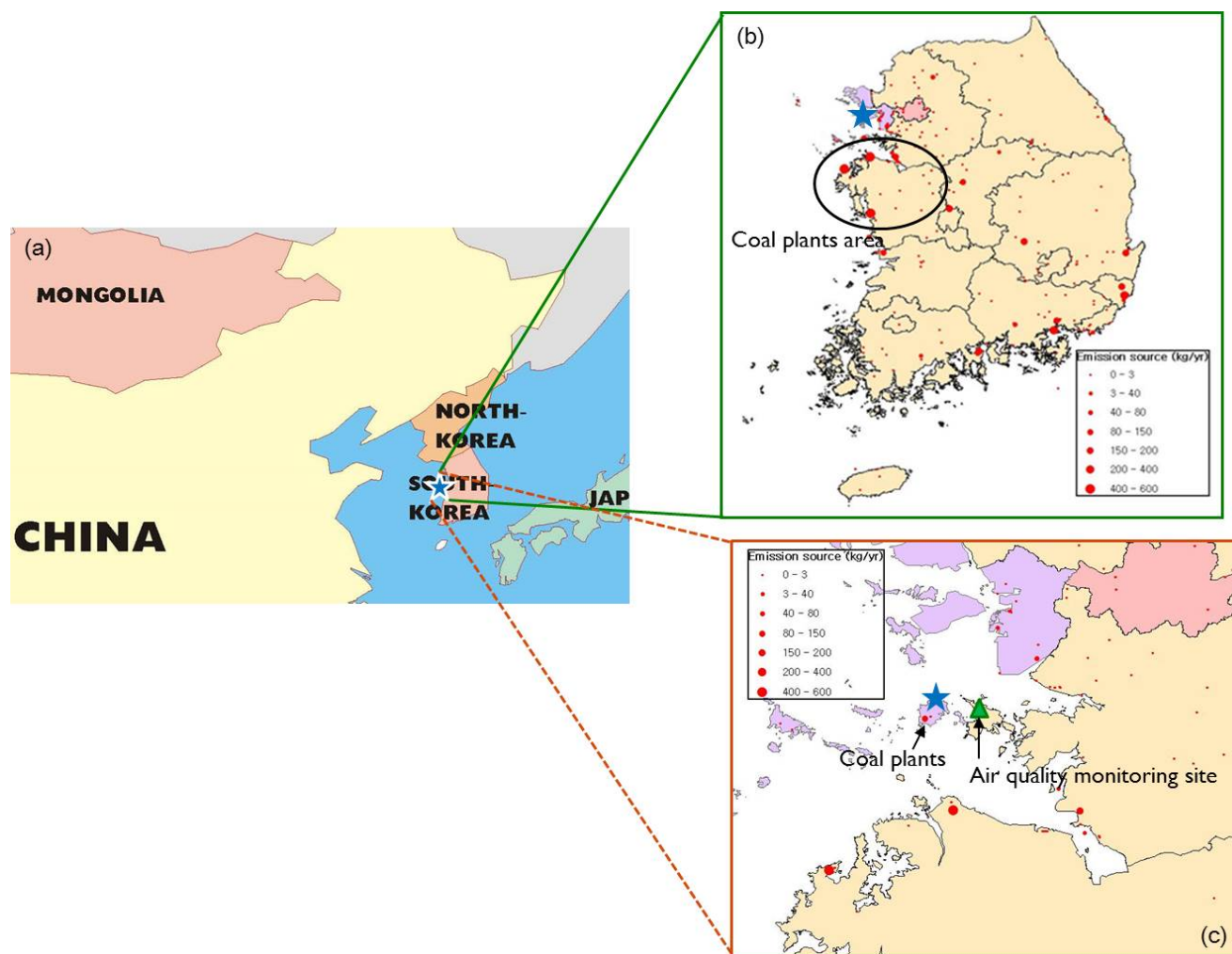


Figure 1. (a) The sampling site in Yongheung Island (the star mark). (b) Anthropogenic mercury emission sources in Korea. Blue star indicates the sampling site, and the green circle indicates the area where major Korean coal-fired power plants are located. (c) The enlarged image of the area near the sampling site.

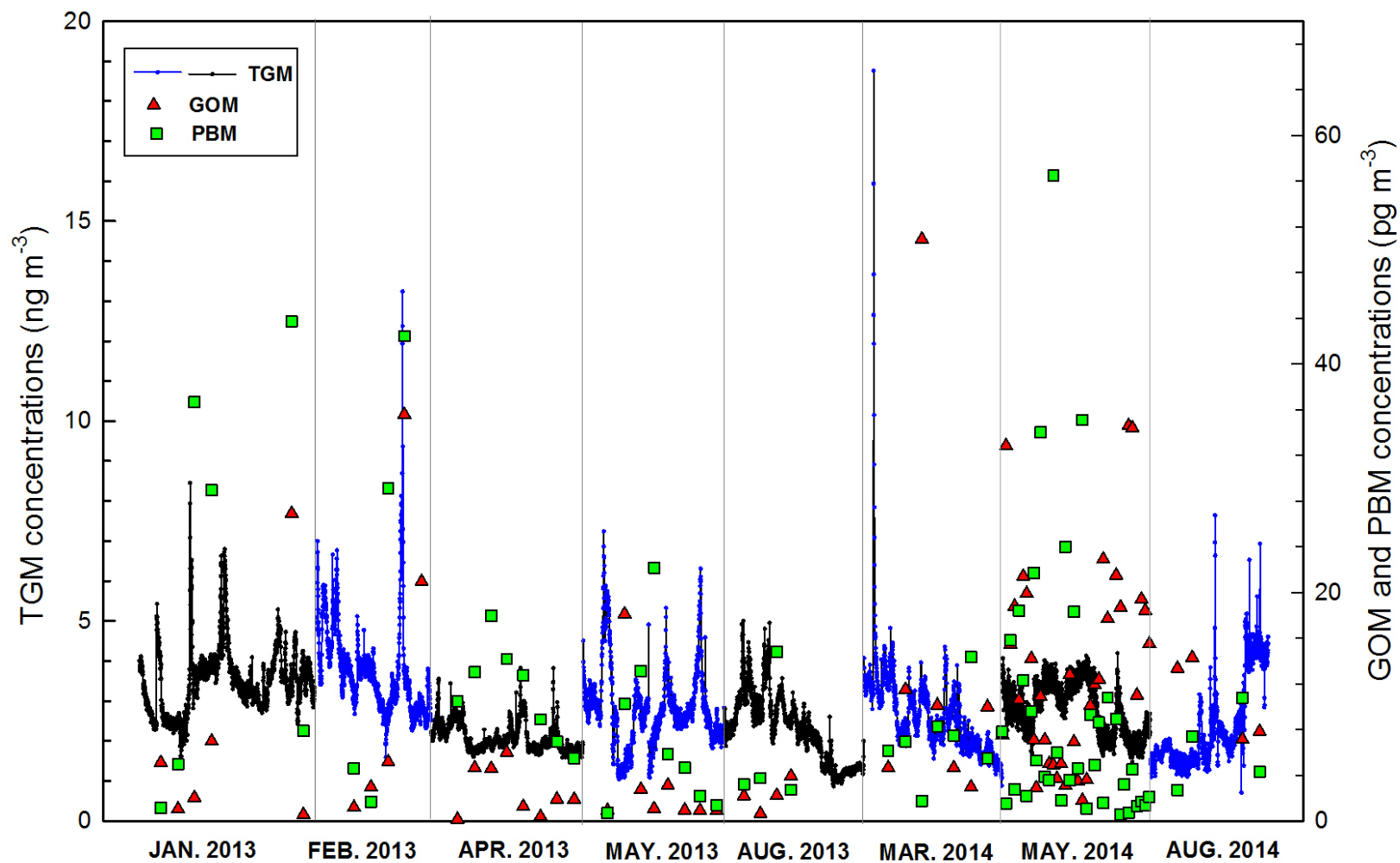


Figure 2. TGM, GOM, and PBM concentrations measured during the eight sampling periods. TGM was measured every 5 minutes while GOM and PBM were measured during 12hrs except for the 2hr measurements during May, 2014.

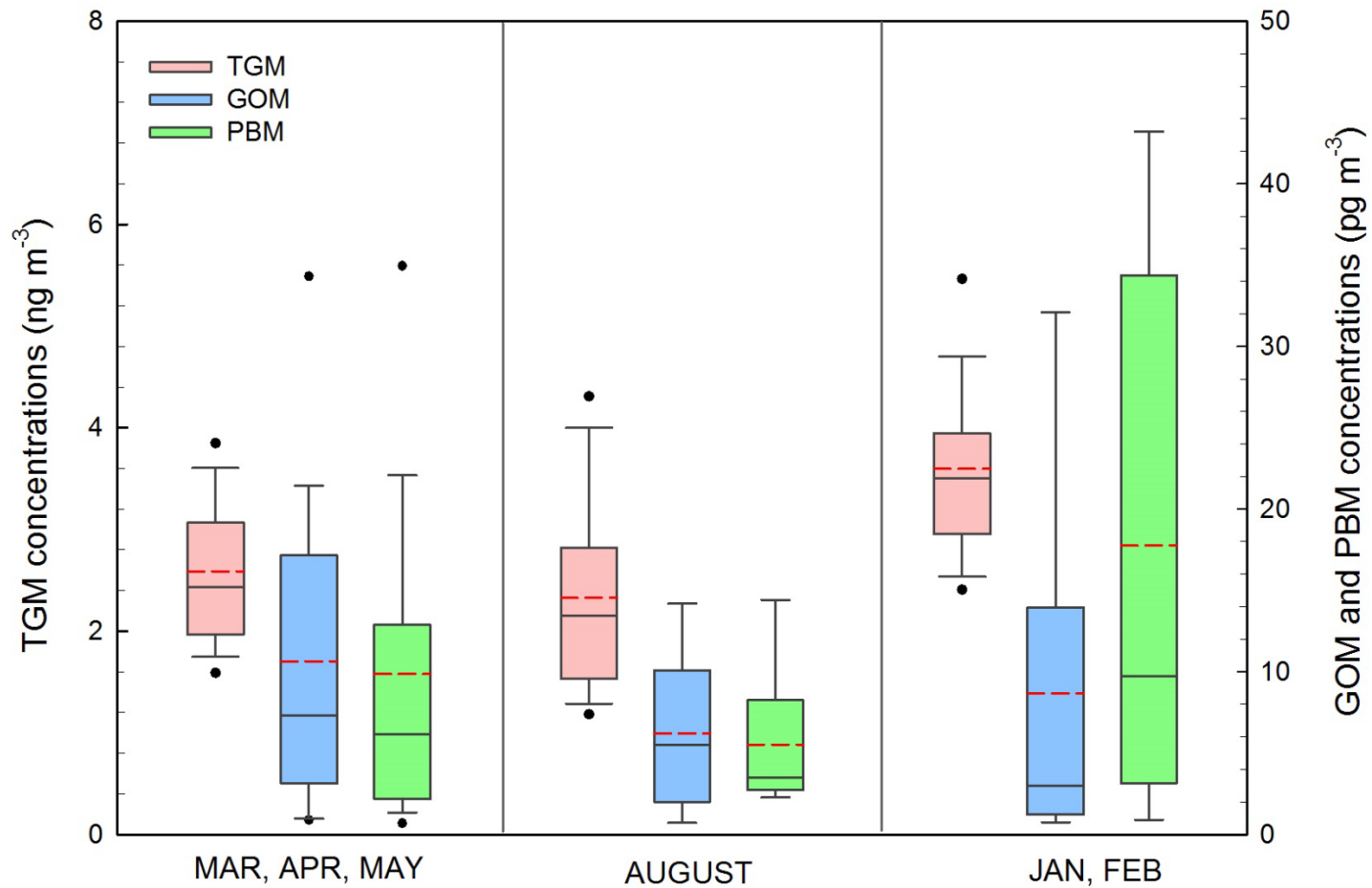


Figure 3. Box-and-whisker plot for the concentrations of TGM, GOM, and PBM during three different periods. The red dash lines indicate the arithmetic mean.

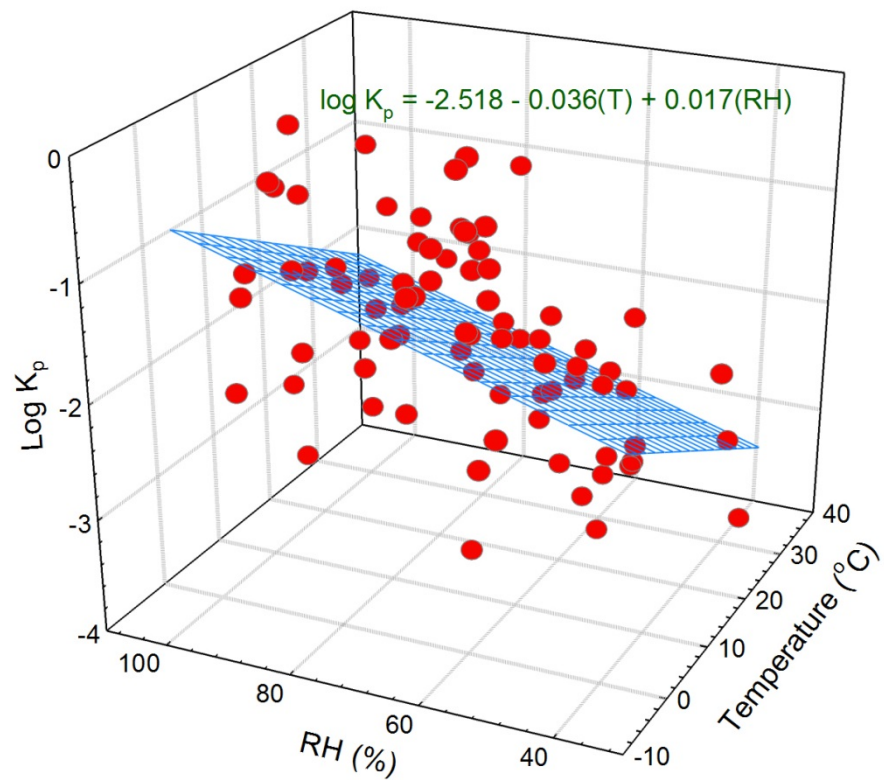


Figure 4. The gas-particle partitioning coefficient, K_p , related to atmospheric temperature and relative humidity (RH) (n=81).

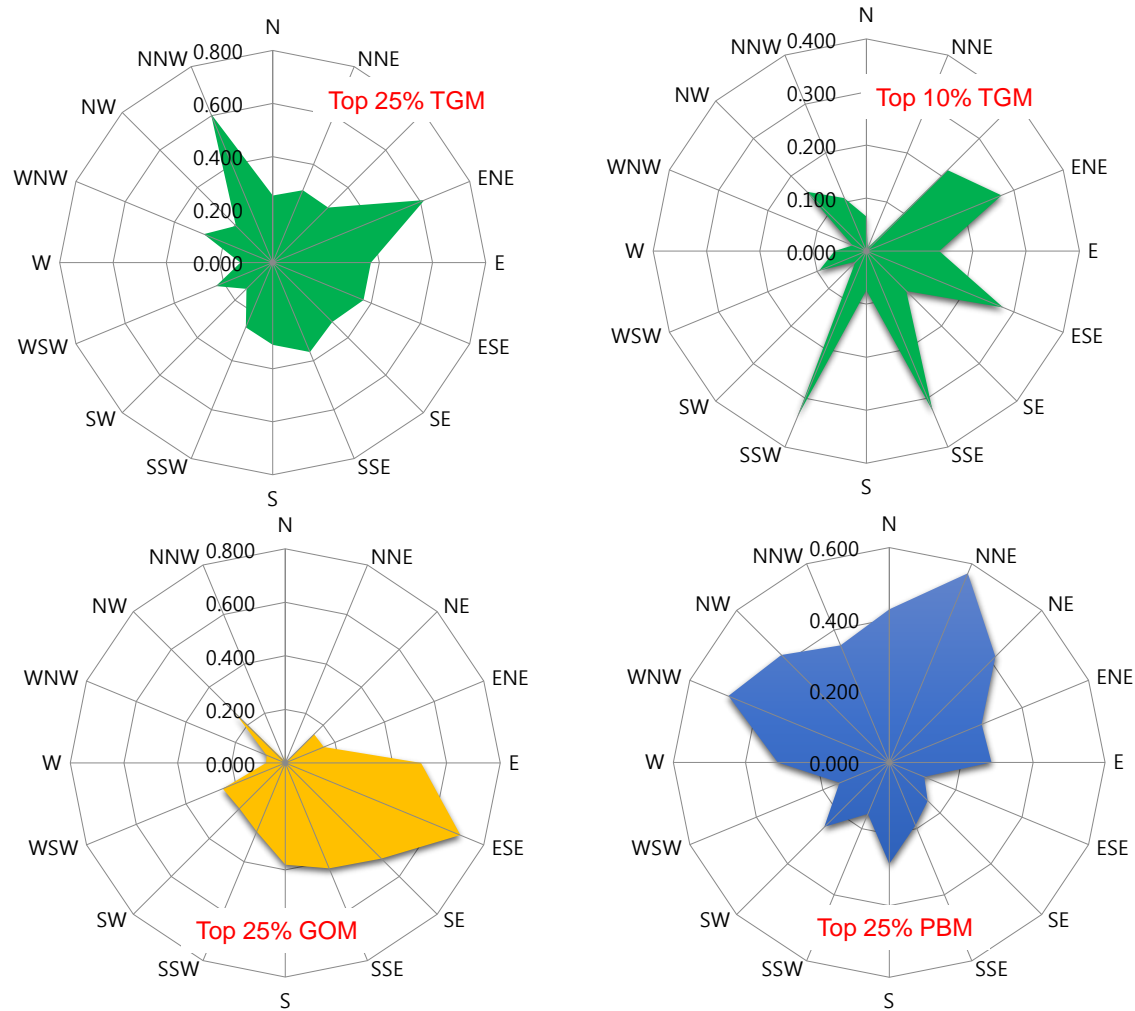


Figure 5. CPF plots for TGM using the top 25% (left upper panel) and the top 10% (right upper panel) as a criterion, and for GOM (left bottom panel) and for PBM (right bottom panel). For both GOM and PBM, the criterion of the top 25% concentration was used.

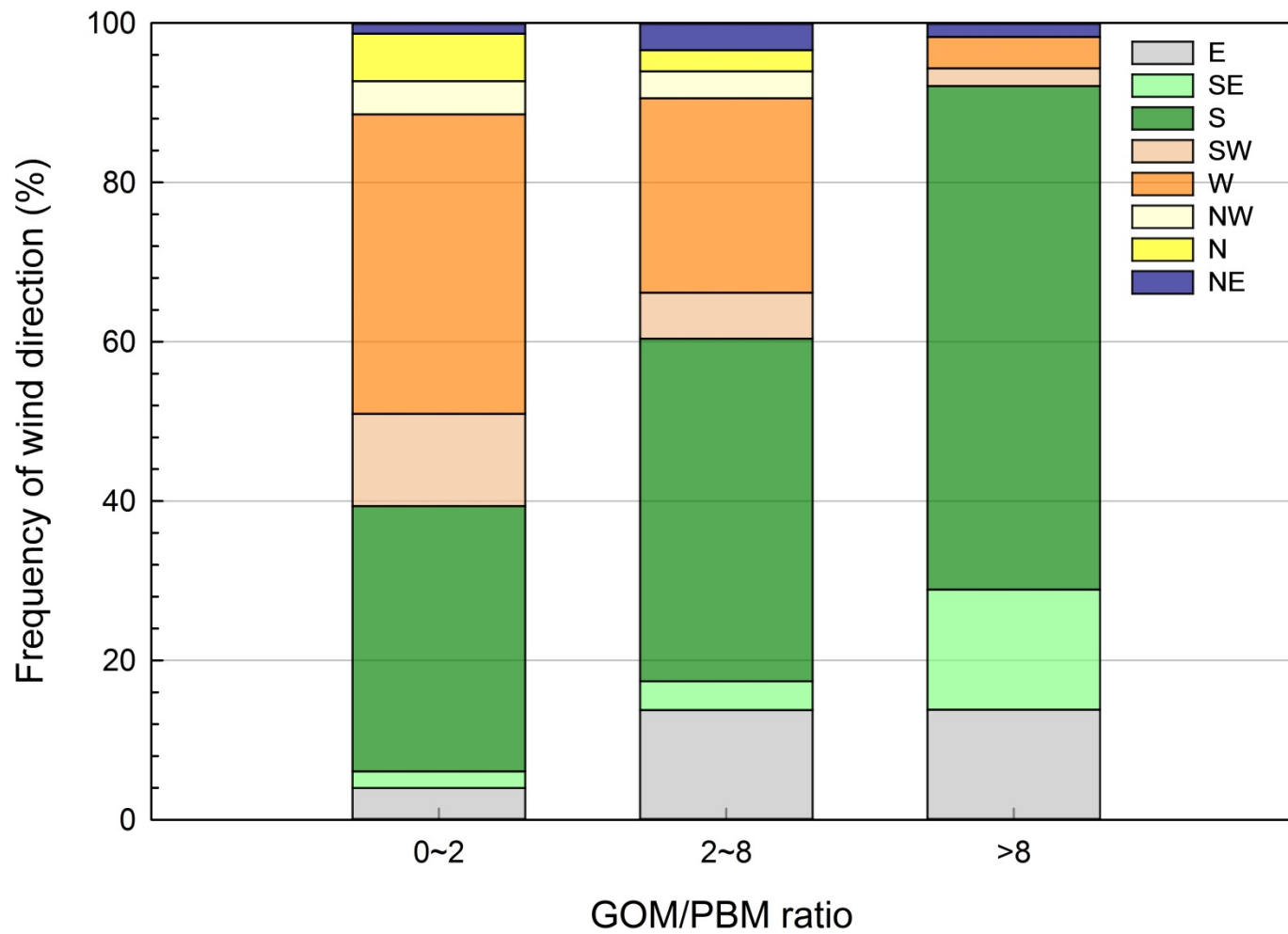


Figure 6. Frequency of wind direction with different GOM/PBM ratios. Southerly and easterly winds prevailed for the samples with high GOM/PBM ratio whereas the percentage of westerly winds increased as the GOM/PBM ratio decreased.

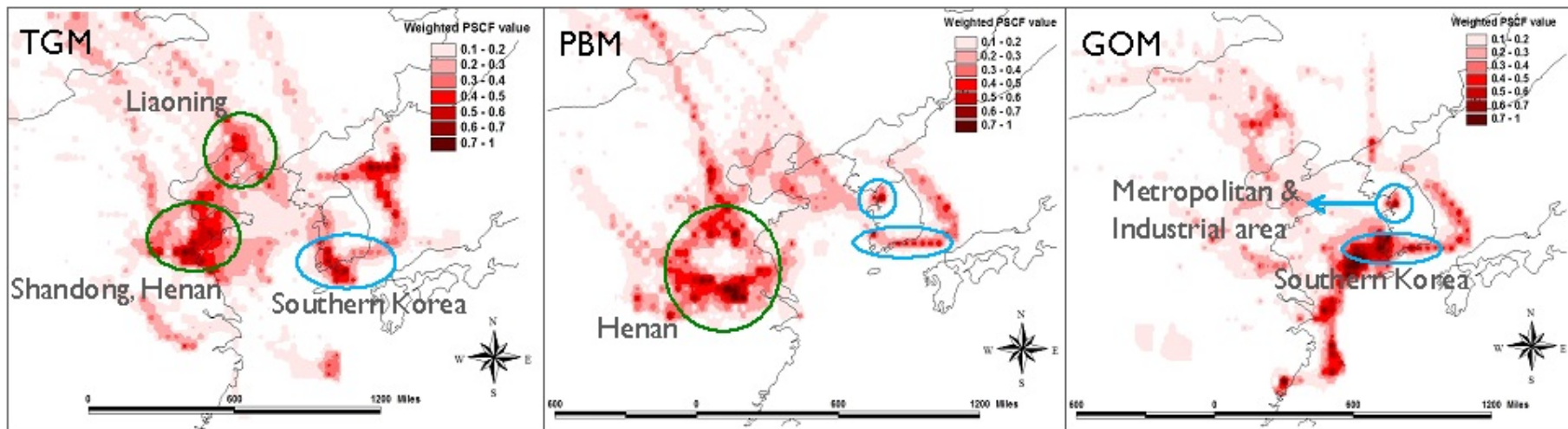


Figure 7. PSCF results for TGM (left), PBM (middle), and GOM (right) using the top 25% of concentrations as criteria.

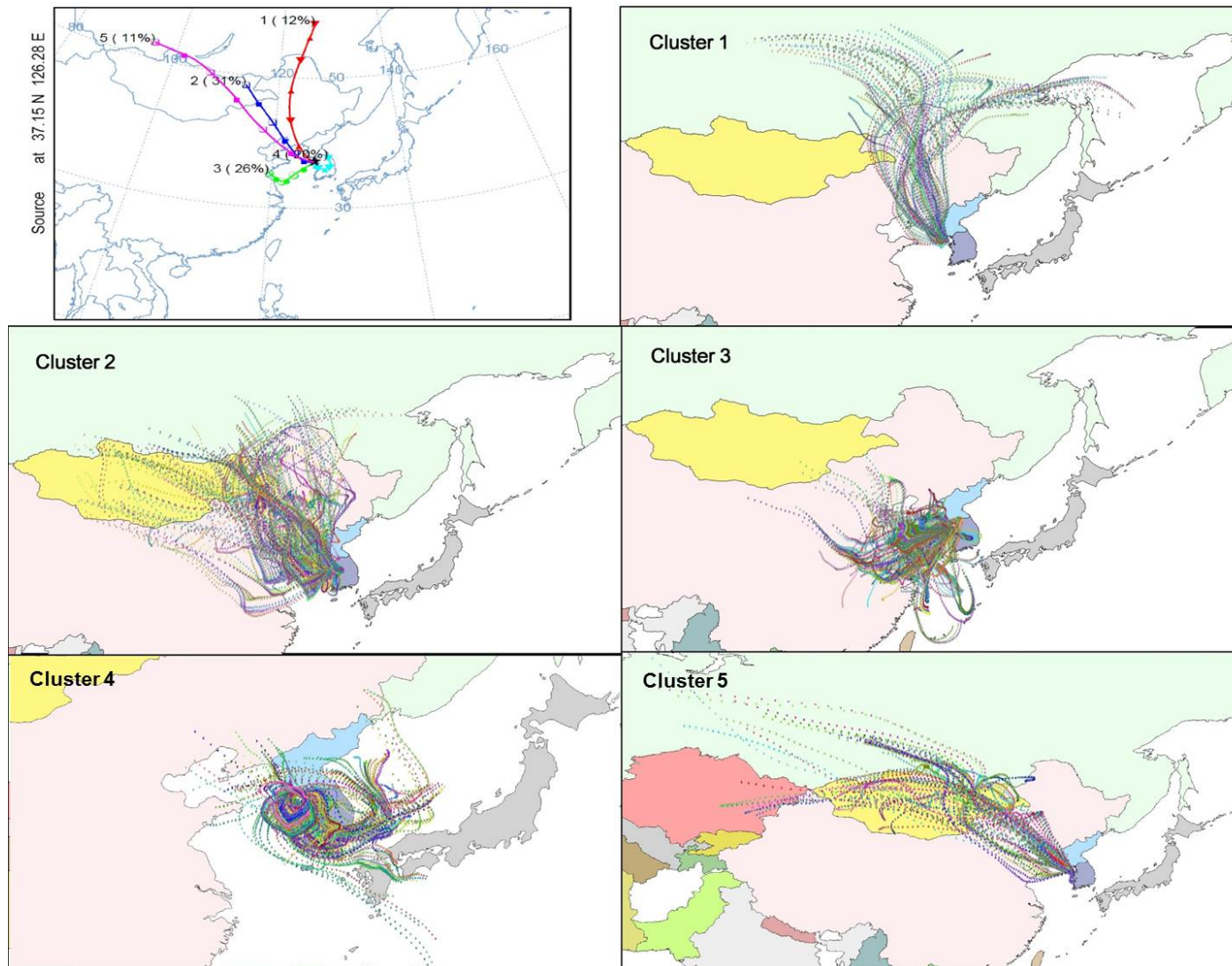


Figure 8. Back-trajectories for clusters 1 through 5. The left top panel indicates the mean back-trajectory and contribution for each cluster.